Scientific Research Publishing

Journal of Applied Mathematics and Physics, 2023, 11, 1113-1123
https://www.scirp.org/journal/jamp
ISSN Online: 2327-4379
ISSN Print: 2327-4352

# First Principles Investigation of the Structure and Properties of Superconducting Cubic Protactinium Hydride $PaH_3$

**Tao Liu[1*], Tao Gao[2]**

[1]School of Electronic and Communication Engineering, Guiyang University, Guiyang, China
[2]Institute of Atomic and Molecular Physics, Sichuan University, Chengdu, China
Email: *liutao_july@163.com

**How to cite this paper:** Liu, T. and Gao, T. (2023) First Principles Investigation of the Structure and Properties of Superconducting Cubic Protactinium Hydride $PaH_3$. *Journal of Applied Mathematics and Physics*, **11**, 1113-1123.
https://doi.org/10.4236/jamp.2023.114073

**Received:** March 29, 2023
**Accepted:** April 25, 2023
**Published:** April 28, 2023



## Abstract

Cubic protactinium hydrides are very important existing form in superconducting protactinium hydrogen series. In this work, the ground state structure and properties of cubic $PaH_3$ have been studied using the DFT + $U$ method. This systematic study for two bulk properties includes the electronic structures, phonon dispersion curves, structural, mechanical and thermodynamic properties under the effective coulomb $U$ and exchange $J$ PBE + $U$ parameters. Structural relaxation results show that the Pa–H and Pa–Pa distances in $\alpha$-$PaH_3$ are significantly higher than that in $\beta$-$PaH_3$, and the H–H distances in $\alpha$-$PaH_3$ are slightly smaller than that in $\beta$-$PaH_3$. For the ground state electronic structures of $\alpha$-$PaH_3$ and $\beta$-$PaH_3$, we found that $\alpha$-$PaH_3$ and $\beta$-$PaH_3$ are metallic, and the protactinium 5$f$ electronic states and hydrogen have obvious bonding effect, resulting in weakening of the material's metallicity. This is consistent with observations for the other actinide hydrides such as $ThH_3$ and $UH_3$. The phonon spectrum calculations reveal that the PBE and PBE + $U$ methods give quite different frequencies for the optical branches of phonons of $\alpha$-$PaH_3$ and $\beta$-$PaH_3$. In addition, by including the vibrational entropy and the ZPE using the phonon frequencies obtained from the optimized unit cells we predict that the $\beta$-$PaH_3$ phase can not transit into $\alpha$-$PaH_3$ phase above room temperature.

## Keywords

$\alpha$-$PaH_3$ and $\beta$-$PaH_3$, Electronic Properties, Mechanical Properties, Thermodynamic Properties, Density Functional Theory (DFT)

## 1. Introduction

In the actinide hydrides series, Thorium (Th), Uranium (U) and Plutonium (Pu)

hydrides have been widely studied due to their important role in the nuclear industry. However, there are few reports on others actinide hydrides such as protactinium hydride (Pa-H). Protactinium hydride has generated some interest because protactinium is considered as a component of the conventional nuclear waste and an opportunity for studying the physics and chemistry of actinide-based materials [1] [2]. Moreover, protactinium hydride shows a variety of structural phases under different pressures. Xiao *et al.* systematically study the structure and superconductivity of protactinium hydride ($PaH_n$) at different pressures using the first principle [3]. Although the cubic $PaH_8$ ($Fm$-3$m$) exhibits high superconducting critical transition temperature under high pressure, the cubic $PaH_3$ structure seems to be thermodynamically stable within 100 GPa. Thus, in order to understand the rich structural phases and superconducting properties of protactinium hydride, it is very important to study the ground state structure and physical properties of cubic protactinium hydride.

As early as 1984, Ward *et al.* experimentally reported structures, physical and chemical properties of a solid solution $Pa_3H_4$-$Pa_3H_5$ above 500 K and cubic $PaH_3$ phase for the Pa-H system [2]. Sellers *et al.* reported that metal Pa with $H_2$ reacted at 523 K to form a black $\beta$-$PaH_3$ which was isostructural with cubic $\beta$-$UH_3$ [1]. Dod reported that $\alpha$-$PaH_3$ formed between 373 K and 473 K had a cubic $\alpha$-$UH_3$-type structure [2]. Moreover, these early studies indicated that Pa-H system shows some similarities with U-H system. This also provides signs for further understanding and potential applications of cubic $PaH_3$ phase. The neighbouring thorium-hydrides (Th-H) and uranium-hydrides (U-H) systems have been thoroughly investigated [4] [5] [6] [7] and each exhibits unique properties, but the ground state structures and properties of the cubic $PaH_3$ are not known.

John W. Ward [2] reported that the high temperature phase $\beta$-$PaH_3$ transits irreversibly into the low temperature phase $\alpha$-$PaH_3$ above room temperature. Based on the irreversibility of the $\beta$ to $\alpha$ phase transition, $\alpha$-$PaH_3$ is always believed to be a metastable state. To further understand the phase transition process, the ground state properties such as structures, phonon spectrum, electronic, mechanical and thermodynamic properties of cubic $PaH_3$ phase should be supplied. For actinide-based compounds, the density functional theory (DFT) schemes including the local spin density approximation (LSDA) or the generalized gradient approximation (GGA) fail to get the ground state, while the DFT + $U$ formalisms can effectively get the right ground state such as its neighbor thorium and uranium compounds [8] [9] [10] [11]. Considering that 5$f$ electronic states of cubic $PaH_3$ system show both localized and itinerant characters [2], here we present a comparative DFT + $U$ study on the ground-state properties of $\alpha$-$PaH_3$ and $\beta$-$PaH_3$.

## 2. Computational Details

In our works, all DFT calculations are performed using the Vienna Ab initio Simulation Package (VASP, version 5.4) [12] [13]. The exchange-correlation functional in the local density approximation (LDA) and the generalized gra-

dient approximation (GGA) as parametrized by Perdew-Burke-Ernzerhof (PBE) [14] [15] were used in this study. A Hubbard-like term was added in order to take into account the strong 5*f* electron correlations in actinide protactinium cation, according to the DFT + *U* scheme. The brillouin zones were divided using Monchhorst Pack *k*-mesh with 9 × 9 × 9 grid for the DFT + *U* calculations. The kinetic energy cut off of 550 eV was used for plane waves. The energy convergence criterion was $10^{-6}$ eV. The Hellmann-Feynman forces on each atom for ionic relaxation were less than 0.01 eV/Å. The DFT + *U* approach [16] [17] [18] [19] [20] was carried out to enforce localization of Pa 5*f* electrons. The total energy functional for this scheme is of the form

$$E_{DFT+U} = E_{DFT} + \frac{U-J}{2}\sum_{\sigma}\left[Tr\rho^{\sigma} - Tr\left(\rho^{\sigma}\rho^{\sigma}\right)\right] \quad (1)$$

where $\rho^{\sigma}$ is the density matrix of Pa-*f* states, *U* and *J* are the spherically averaged screened coulomb energy and exchange energy, respectively.

## 3. Results and Discussion

### 3.1. Structural and Mechanical Properties

The crystal structures of $\alpha$-$PaH_3$ and $\beta$-$PaH_3$ have been shown in **Figure 1(a)** and **Figure 1(b)** respectively. The different magnetic orders (*i.e.* FM and AFM) are adopted in our DFT + *U* calculations. In the meanwhile, for $\alpha$-$PaH_3$ and $\beta$-$PaH_3$, the relationship between the optimized lattice constant and a series of *U* values is shown in **Figure 2(a)** and **Figure 2(b)** respectively. Our LDA/PBE + *U* calculated results show that there is no obvious difference between the effect of ferromagnetic and antiferromagnetic order on the lattice parameters of cubic $\alpha$-$PaH_3$ and $\beta$-$PaH_3$. In **Figure 2(a)**, when the *U* is around 2.0 eV, our calculated lattice constant of $\alpha$-$PaH_3$ using the PBE + *U* method is good calculation result compared to experimental data. However, as shown in **Figure 2(b)**, our results for FM phase of $\beta$-$PaH_3$ demonstrates that the lattice constant is close to the experimental value [1] [2] when *U* is around 4.0 eV. Thus, for cubic $\alpha$-$PaH_3$ and $\beta$-$PaH_3$, the lattice constants obtained from the PBE + *U* computations are in good agreement with the experimental data.

In **Table 1**, the lattice constant and the interatomic distance of $\alpha$-$PaH_3$ and $\beta$-$PaH_3$ using the PBE and PBE + *U* methods were listed. Our structural relaxation results show that the atomic spacing has obvious difference in $\alpha$-$PaH_3$ and $\beta$-$PaH_3$ structures. In $\alpha$-$PaH_3$, the Pa–H distance is 2.305 Å, significantly higher than the Pa–H distance in $\beta$-$PaH_3$. Moreover, the Pa–H distance in $\beta$-$PaH_3$ is also higher than that in $\alpha$-$PaH_3$ structure. Charge density decomposition using the Bader method suggests that the Pa atoms forming linear chains in $\beta$-$PaH_3$ atoms are bonded: the bond-lengths of 2.555 Å are only slightly larger than the largest nearest-neighbor distance in the metallic Pa phase (0.326 nm). Therefore, the calculated results show that the Pa–H and Pa–Pa distances in $\alpha$-$PaH_3$ is significantly higher than that in $\beta$-$PaH_3$, and the H–H distances in $\alpha$-$PaH_3$ is slightly smaller than that in $\alpha$-$PaH_3$.

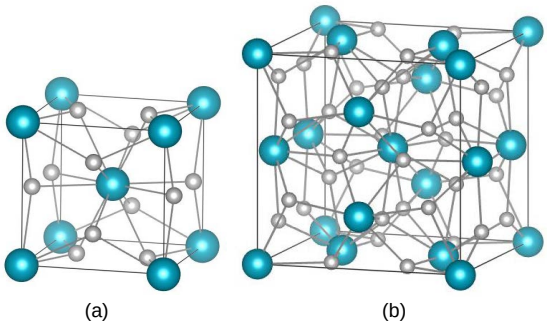


**Figure 1.** Cubic $PaH_3$ structure: $\alpha$-$PaH_3$ (a) and $\beta$-$PaH_3$ (b), where the large and small balls denote the protactinium and hydrogen atoms, respectively.

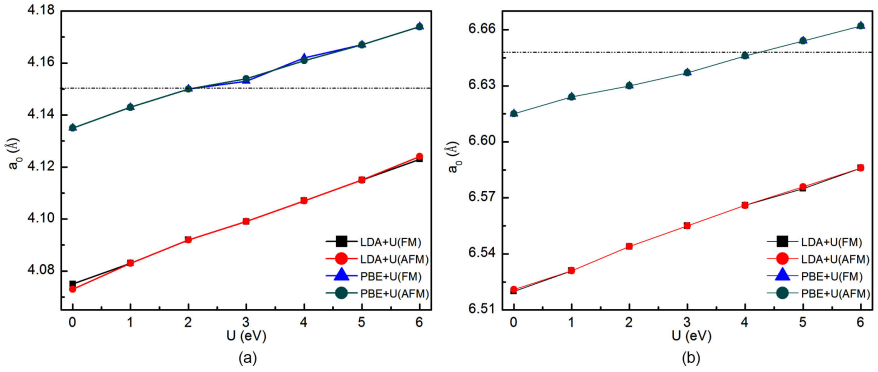


**Figure 2.** Optimized lattice parameter for $\alpha$-$PaH_3$ (a) and $\beta$-$PaH_3$ (b) in LDA/PBE + $U$ as a function of the parameter $U$.

**Table 1.** The lattice constant and interatomic distance for $\alpha$-$PaH_3$ and $\beta$-$PaH_3$.

| Compound | Method | $a_0$ (Å) | $d$(Pa–H) (Å) | $d$(Pa–Pa) (Å) | $d$(H–H) (Å) |
|---|---|---|---|---|---|
| $\alpha$-$PaH_3$ | PBE | 4.135 | 2.288 | 4.093 | 2.047 |
| | PBE + $U$ | 4.149 | 2.305 | 4.123 | 2.061 |
| | Expt.[1] [2] | 4.150 | | | |
| $\beta$-$PaH_3$ | PBE | 6.615 | 2.250 | 3.276 | 2.537 |
| | PBE + $U$ | 6.646 | 2.261 | 3.294 | 2.555 |
| | Expt.[2] | 6.648 | | | |

In **Table 2**, the elastic constants, bulk modulus, shear modulus, Young's modulus and Poisson's ratio of $\alpha$-$PaH_3$ and $\beta$-$PaH_3$ using the PBE and PBE + $U$ methods were listed. For cubic $\alpha$-$PaH_3$ and $\beta$-$PaH_3$ structures, the elastic constants satisfy the following mechanical stability criteria [21]:

$$C_{11} > 0,\ \ C_{44} > 0,\ \ C_{11} > \left|C_{12}\right|,\ \ \left(C_{11} + 2C_{12}\right) > 0 \tag{2}$$

These results indicate that the structure of $\alpha$-$PaH_3$ and $\beta$-$PaH_3$ is stable. We have calculated the bulk ($B$) and shear moduli ($G$), Young's modulus ($E$) and Poisson's ratio ($\upsilon$) of $\alpha$-$PaH_3$ and $\beta$-$PaH_3$ using the Voigt-Reuss-Hill (VRH) approximations [22] [23]. From **Table 2**, the obtained bulk and shear moduli of

**Table 2.** The calculated elastic constants $C_{ij}$, bulk modulus $B$, shear modulus $G$, Young's modulus $E$ and Poisson's ratio $\upsilon$ for $\alpha$-$PaH_3$ and $\beta$-$PaH_3$. The elastic constants and moduli are in units of GPa.

| Compound | Methods | $C_{11}$ | $C_{12}$ | $C_{44}$ | $B$ | $G$ | $E$ | $\upsilon$ |
|---|---|---|---|---|---|---|---|---|
| $\alpha$-$PaH_3$ | PBE | 316.29 | 51.40 | 28.87 | 139.70 | 49.08 | 131.80 | 0.34 |
| | PBE + $U$ | 309.66 | 70.14 | 28.26 | 149.98 | 44.00 | 120.24 | 0.37 |
| $\beta$-$PaH_3$ | PBE | 195.48 | 79.53 | 51.94 | 118.18 | 39.02 | 105.45 | 0.35 |
| | PBE + $U$ | 227.97 | 76.72 | 39.81 | 127.14 | 38.62 | 105.21 | 0.36 |

$\alpha$-$PaH_3$ and $\beta$-$PaH_3$ with the PBE+ $U$ are larger than that the PBE. These differences might be owing to the overestimation of lattice constants by PBE + $U$ method. Our obtained Poisson's ratio of 0.34 - 0.37 for $\alpha$-$PaH_3$ and $\beta$-$PaH_3$ is reasonable for being in the range of 0.2 - 0.4 for typical metallic materials.

### 3.2. Electronic Properties

The total density of states (DOS) and projected density of states (PDOS) of $\alpha$-$PaH_3$ and $\beta$-$PaH_3$ are shown in **Figure 3** by using the PBE and PBE + $U$ methods. **Figure 3** shows the protactinium 5$f$ electrons are mainly distributed and there is no obvious localization feature at the Fermi energy for the electronic structure of $\alpha$-$PaH_3$ and $\beta$-$PaH_3$. Although the 5$f$ electron of Pa in these two systems is a strongly electronic correlation effects, Pa-$f$ and H-$s$ electrons have obvious hybrid effect near the Fermi energy level, and further proves that the protactinium 5$f$ electrons have itinerant characters in $\alpha$-$PaH_3$ and $\beta$-$PaH_3$. In cubic $PaH_3$ structure, Pa 5f electrons does not show strong localization characteristics near the Fermi level, but has obvious bonding effect with Hand H 1s electrons. This is very similar to the electronic properties of protactinium hydride ($PaH_n$) (n = 1 - 9) in $Fm\bar{3}m$-$PaH_8$ superconductive structure studied by Xiao *et al.* [3]. Thus, for cubic $\alpha$-$PaH_3$ and $\beta$-$PaH_3$, the electronic properties for Pa-f and H-s are very important for the superconductivity of Pa-H system.

As shown in **Figure 4**, the difference charge density distribution is further analyzed for $\alpha$-$PaH_3$ and $\beta$-$PaH_3$, to study the bonding characters between protactinium and hydrogen atoms. We can see clearly that the ionic character of the protactinium-hydrogen bonds is enhanced with the PBE + $U$ formalism. This result is in consistent with our previous PDOS analysis.

### 3.3. Phonon Spectrum and Thermodynamic Properties

Phonon frequency and thermodynamic properties calculations are carried out using the Hellmann-Feynman theorem and the supercell method [24]. A 2 × 2 × 2 supercell is adopted to calculate the force constants, and a 3 × 3 × 3 Monkhorst-Pack $k$-points mesh is used for integrations over the BZ. The atomic displacements for force constants calculations are all set to 0.02 Å.

For $\alpha$-$PaH_3$ and $\beta$-$PaH_3$, the phonon dispersion curves in the BZ and together with the phonon DOS are shown in **Figure 5(a)** and **Figure 5(b)**. For cubic

$PaH_3$, the acoustic and optical branches of phonon come from Pa and H vibrations, and Pa atoms are much heavier than H atoms, thus a large gap between acoustic and optical branches can be observed. For the three acoustic branches, the dispersion curves are almost the same in PBE and PBE + $U$ results. While for the optical branches from Figure 5(a), the frequencies calculated with PBE + $U$ are all shifted down by about 2.3 THz that in comparison with PBE. This is because the on-site Coulomb repulsion enhances the ionic character of the Pa-H bonds, and thus reduces the bonding strength. Our studies indicate that the lattice dynamics behaviors of both $\alpha$- and $\beta$-$PaH_3$ strongly depend on the electronic correlation effects.

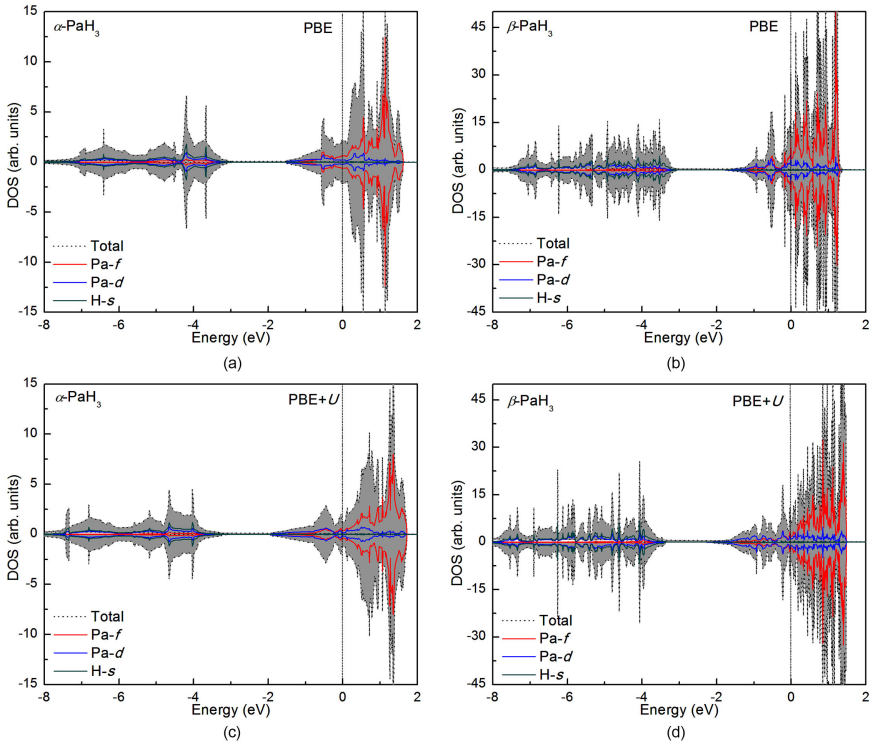


Figure 3. Total and projected electronic density of states (DOS) of $\alpha$-$PaH_3$ and $\beta$-$PaH_3$ using PBE and PBE + $U$ method.

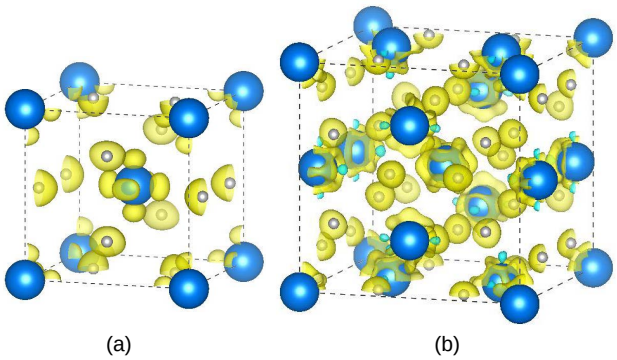


Figure 4. Difference electron charge density of $\alpha$-$PaH_3$ (a) and $\beta$-$PaH_3$ (b) using the PBE + $U$ method.

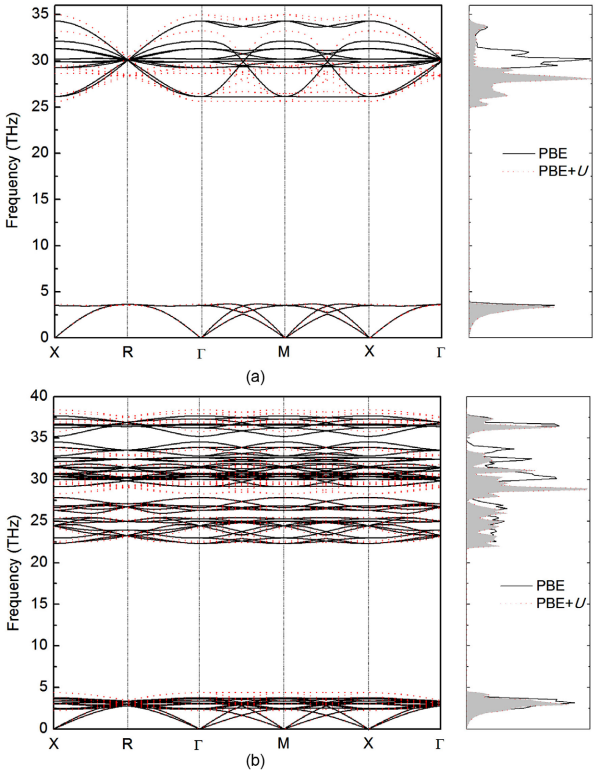


**Figure 5.** Phonon dispersion curves (left panel) and corresponding phonon DOS (right panel) of $\alpha$-$PaH_3$ (a) and $\beta$-$PaH_3$ (b) using the PBE and PBE + $U$ method.

The thermodynamic properties such as the Helmholtz free energy $F$, vibrational entropy $S$, vibrational energy $E$, the heat capacity $C_v$ (**Figure 6**) and the zero point energy (ZPE, **Table 3**) have been calculated by the density functional perturbation theory (DFPT) [25] [26]. All these properties are expressed per $\alpha$-$PaH_3$ and $\beta$-$PaH_3$ unit, and a sample of values at 300 and 500 K is presented in **Table 3**. For $\alpha$-$PaH_3$ and $\beta$-$PaH_3$, the vibrational energy $E$ exhibits a similar trend that increases almost linearly with temperature and tends to display $k_BT$ behavior at high temperatures. With the increase of temperature, the differences between $\alpha$-$PaH_3$ and $\beta$-$PaH_3$ becomes even more apparent, which may be attributed to the higher frequencies related to lighter H atom vibrations. And the $F$ decreases almost linearly with temperature. The entropy $S$ increases with the rising of temperature since the vibrational contribution to the entropy increases as the temperature rises. However, **Figure 6(b)** demonstrates the entropy of $\beta$-$PaH_3$ is significantly higher than that of $\alpha$-$PaH_3$, the discrepancies are mainly because of the difference in the number of hydrogen atoms. In addition, the heat capacity $C_v$ increases with the applied temperature. Below a temperature of around 200 K, the $C_v$ increases very rapidly with increasing temperature and displays the $T^3$ law behavior. And above 800 K, the $C_v$ increases slowly with temperature and gradually approaches the Dulong-Petit limit [27]. Hence, the $\beta$ phase of cubic $PaH_3$ may not transit into $\alpha$ phase above room temperature owing to the thermodynamic criteria.

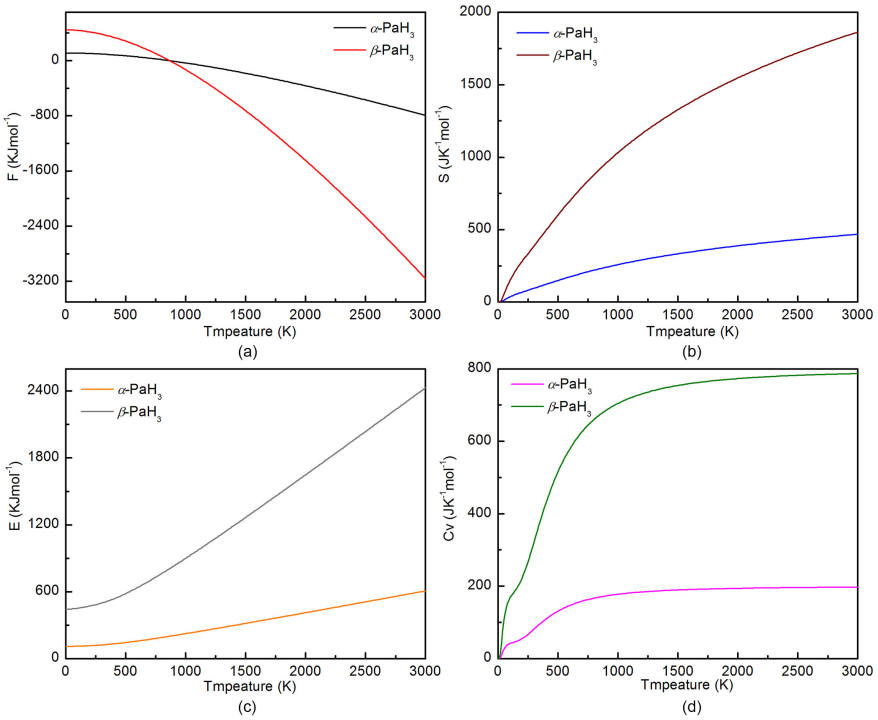


**Figure 6.** Thermodynamic properties of $\alpha$-$PaH_3$ and $\beta$-$PaH_3$ using the PBE + $U$ method: the Helmholtz free energy $F$ (a), the entropy $S$ (b), the internal energy $E$ (c), and the constant-volume specific heat $C_v$ (d).

**Table 3.** Predicted thermodynamic properties for $\alpha$-$PaH_3$ and $\beta$-$PaH_3$ phases at 300 $K$ and 500 $K$.

| Phase | $T(K)$ | $F_{vib}$ $J/(K{\cdot}mol)$ | $S_{vib}$ $J/mol$ | $C_V$ $J/(K{\cdot}mol)$ | $E_{vib}$ $kJ/mol$ | ZPE $kJ/mol$ |
|---|---|---|---|---|---|---|
| $\alpha$-$PaH_3$ | 300 | 93.10 | 95.10 | 80.98 | 121.63 | 107.96 |
| | 500 | 68.65 | 149.11 | 130.95 | 143.21 | |
| $\beta$-$PaH_3$ | 300 | 381.69 | 386.39 | 321.21 | 497.61 | 442.62 |
| | 500 | 282.99 | 599.28 | 515.32 | 582.63 | |

## 4. Conclusion

In summary, we have systematically studied the structural, electronic, mechanic and thermodynamic properties of $\alpha$-$PaH_3$ and $\beta$-$PaH_3$ by employing the PBE and PBE + $U$ methods. Firstly, to obtain reliable ground state structure and properties of $\alpha$-$PaH_3$ and $\beta$-$PaH_3$ we found the effective $U$ parameter. Then, the Pa–H and Pa–Pa distances in $\alpha$-$PaH_3$ are significantly higher than that in $\beta$-$PaH_3$, and the H–H distances in $\alpha$-$PaH_3$ are slightly smaller than that in $\beta$-$PaH_3$. Moreover, we found that $\alpha$-$PaH_3$ and $\beta$-$PaH_3$ are metallic, and the protactinium 5$f$ electronic states and hydrogen have obvious bonding effect. These studies on the ground state structure and properties of cubic $PaH_3$ system are crucial for further understanding and studying the superconducting properties of metal hydride. Especially for the cubic $PaH_3$, the weak bonding between Pa

and H near the Fermi level provides a useful supplement to the understanding of superconductivity. As a result of effecting the Pa-H bonds, inclusion of the on-site Coulomb interaction largely influences the optical branches of vibration modes for $\alpha$-$PaH_3$ and $\beta$-$PaH_3$. We thus suggest that measuring the vibrational or thermodynamic properties may give out information on the correlation strengths of uranium 5*f* electrons in $\alpha$- and $\beta$-$PaH_3$. Furthermore, the calculations show that the $\beta$-$PaH_3$ phase can not transit into $\alpha$-$PaH_3$ phase above room temperature.

## Acknowledgements

The authors thank Doc. Shiyin Ma for useful discussion.

## Conflicts of Interest

The authors declare no conflicts of interest regarding the publication of this paper.

## References

[1] Sellers, P.A., Fried, S., Elson, R.E., Zachariasen, W. (1954) The Preparation of Some Protactinium Compounds and the Metal. *Journal of the American Chemical Society*, **76**, 5935-5938. https://doi.org/10.1021/ja01652a011

[2] Ward, J.W., Haschke, J.M., Rebizant, J., Bartscher, W. (1984) Phase Relations, Structures and Bonding for the Pa-H System. J*ournal of the Less Common Metals*, **100**,195-214. https://doi.org/10.1016/0022-5088(84)90064-X

[3] Xiao, X., Duan, D., Xie, H., Shao, Z., Li, D., Tian, F., Song, H., Yu, H., Bao, K., Cui, T. (2019) Structure and Superconductivity of Protactinium Hydrides under High Pressure. *Journal of Physics*: *Condensed Matter*, **31**, Article ID: 315403. https://doi.org/10.1088/1361-648X/ab1d03

[4] Rundle, R.E. (1947) The Structure of Uranium Hydride and Deuteride1. *Journal of the American Chemical Society*, **9**, 1719-1723. https://doi.org/10.1021/ja01199a043

[5] Flotow, H.E., Haschke, J.M. and Yamauchi, S. (1984) The Chemical Thermodynamics of Actinide Elements and Compounds: Pt. 9. The Actinide Hydrides. International Atomic Energy Agency, Vienna.

[6] Zachariasen, W.H. (1953) Crystal Chemical Studies of the 5*f*-Series of Elements. XIX. The Crystal Structure of the Higher Thorium Hydride, $Th_4H_{15}$. *Acta Crystallographica*, **6**, 390-393. https://doi.org/10.1107/S0365110X53001095

[7] Peterson, D.T. and Rexer, J. (1962) The Composition of $ThH_2$ and Diffusion of Hydrogen in $ThH_2$. *Journal of the Less Common Metals*, **4**, 92-97. https://doi.org/10.1016/0022-5088(62)90063-2

[8] Devey, A.J. (2011) First Principles Calculation of the Elastic Constants and Phonon Modes of $UO_2$ Using GGA + *U* with Orbital Occupancy Control. *Journal of Nuclear Materials*, **12**, 301-307. https://doi.org/10.1016/j.jnucmat.2011.03.012

[9] Dorado, B., Amadon, B., Freyss, M., Bertolus, M. (2009) DFT + *U* Calculations of the Ground State and Metastable States of Uranium Dioxide. *Physical Review B*, **79**, Article ID: 235125. https://doi.org/10.1103/PhysRevB.79.235125

[10] Chen, Q., Lai, X., Tang, T., Bai, B., Chu, M., Zhang, Y. and Tan, S. (2010) First-Principles Study of the Electronic Structure and Optical Properties of $UO_2$.

*Journal of Nuclear Materials*, **401**, 118-123.
https://doi.org/10.1016/j.jnucmat.2010.04.007

[11] Liu, T., Li, S.C., Gao, T. and Ao, B.Y. (2020) Structural, Electronic, Magnetic and Optical Properties of Protactinium Oxides from Density Functional Theory. *Indian Journal of Physics*, **94**, 53-60. https://doi.org/10.1007/s12648-019-01457-z

[12] Kresse, G. and Hafner, J. (1994) *Ab Initio* Molecular-Dynamics simulation of the Liquid-Metal-Amorphous-Semiconductor Transition in Germanium. *Physical Review B*, **49**, 14251-14269. https://doi.org/10.1103/PhysRevB.49.14251

[13] Kresse, G. and Furthmüller, J. (1996) Efficient Iterative Schemes for *ab Initio* Total-Energy Calculations Using a Plane-Wave Basis Set. *Physical Review B*, **54**, 11169-11186. https://doi.org/10.1103/PhysRevB.54.11169

[14] Perdew, J.P., Ruzsinszky, A., Csonka, G.I., Vydrov, O.A., Scuseria, G.E., Constantin, L.A., Zhou, X. and Burke, K. (2008) Restoring the Density-Gradient Expansion for Exchange in Solids and Surfaces. *Physical Review L*, **100**, Article ID: 136406.
https://doi.org/10.1103/PhysRevLett.100.136406

[15] Hong, J.W., Stroppa, A., Ínigue, J., Picozzi, S. and Vanderbilt, D. (2012) Spin-Phonon Coupling Effects in Transition-Metal Perovskites: a DFT + *U* and Hybrid-Functional Study. *Physical Review B*, **5**, Article ID: 054417.
https://doi.org/10.1103/PhysRevB.85.054417

[16] Dudarev, S.L., Botton, G.A., Savrasov, S.Y., Humphreys, C.J. and Sutton, A.P. (1998) Electron-Energy-Loss Spectra and the Structural Stability of Nickel Oxide: An LSDA + *U* Study. *Physical Review B*, **57**, 1505-1509.
https://doi.org/10.1103/PhysRevB.57.1505

[17] Anisimov, V.I., Zaanen, J. and Andersen, O.K. (1991) Band Theory and Mott Insulators: Hubbard *U* Instead of Stoner. *Physical Review B*, **44**, 943-954.
https://doi.org/10.1103/PhysRevB.44.943

[18] Anisimov, V.I., Aryasetiawan, F. and Lichtenstein, A.I. (1997) First-Principles Calculations of the Electronic Structure and Spectra of Strongly Correlated Systems: the LDA + *U* Method. *Journal of Physics*: *Condensed Matter*, **9**, 767-808.
https://doi.org/10.1088/0953-8984/9/4/002

[19] Liechtenstein, A.I., Anisimov, V.I. and Zaanen, J. (1995) Density-Functional Theory and Strong Interactions: Orbital Ordering in Mott-Hubbard Insulators. *Physical Review B*, **52**, R5467-R5470. https://doi.org/10.1103/PhysRevB.52.R5467

[20] Czyżyk, M.T. and Sawatzky, G.A. (1994) Local-Density Functional and on-Site Correlations: The Electronic Structure of $La_2CuO_4$ and $LaCuO_3$. *Physical Review B*, **9**, 14211-14228. https://doi.org/10.1103/PhysRevB.49.14211

[21] Wu, Z.-J., Zhao, E.-J., Xiang, H.-P., Hao, X.-F., Liu, X.-J. and Meng, J. (2007) Crystal Structures and Elastic Properties of Superhard $IrN_2$ and $IrN_3$ from First Principles. *Physical Review B*, **76**, Article ID: 054115.
https://doi.org/10.1103/PhysRevB.76.054115

[22] Hill, R. (1952) The Elastic Behaviour of a Crystalline Aggregate. *Proceedings of the Physical Society*. *Section A*, **65**, 349-354.
https://doi.org/10.1088/0370-1298/65/5/307

[23] Haines, J., Léger, J.M. and Bocquillon, G. (2001) Synthesis and Design of Superhard Materials. *Annual Review of Materials Research*, **31**, 1-23.
https://doi.org/10.1146/annurev.matsci.31.1.1

[24] Parlinski, K., Li, Z.Q. and Kawazoe, Y. (1997) First-Principles Determination of the Soft Mode in Cubic $ZrO_2$. *Physical Review L*, **78**, 4063-4066.
https://doi.org/10.1103/PhysRevLett.78.4063

[25] Baroni, S., De Gironcoli, S., Dal Corso, A. and Giannozzi, P. (2001) Phonons and Related Crystal Properties from Density-Functional Perturbation Theory. *Reviews of Modern Physics*, **73**, 515-562. https://doi.org/10.1103/RevModPhys.73.515

[26] Gonze, X. (1995) Adiabatic Density-Functional Perturbation Theory. *Physical Review A*, **52**, 1096-1114. https://doi.org/10.1103/PhysRevA.52.1096

[27] Terki, R., Bertrand, G., Aourag, H. and Coddet, C. (2008) Thermal Properties of $Ba_{1-x}Sr_xZrO_3$ Compounds from Microscopic Theory. *Journal of Alloys and Compounds*, **456**, 508-513. https://doi.org/10.1016/j.jallcom.2007.02.133